Crater Formation Mechanism on the Surface of a Biaxially Oriented Polypropylene Film

Satoshi Tamura,[1] Koichi Takino,[2] Toshiro Yamada,[2] Toshitaka Kanai[3]

[1]*Prime Polymer Company, Limited, 580-30, Nagaura, Sodegaura-City, Chiba 299-0265, Japan*
[2]*Kanazawa University, Kakuma-Machi, Kanazawa, Ishikawa 920-1192, Japan*
[3]*Idemitsu Kosan Company, Limited, 1-1, Anesaki-Kaigan, Ichihara-City, Chiba, 299-0193, Japan*

Received 29 August 2011; accepted 12 January 2012
DOI 10.1002/app.36803
Published online 00 Month 2012 in Wiley Online Library (wileyonlinelibrary.com).

ABSTRACT: Biaxially oriented polypropylene (BOPP) films are used in a variety of areas around the world. They are especially well suited for food packaging and industrial usages because of their high productivity. Many studies on the stretchability with regard to crystal structure changes have been reported by various researchers because the machine speed has been increasing and the demand to produce thinner films has been becoming more important. Furthermore, a number of studies on the surface structure of BOPP films with craterlike roughnesses have been reported since the 1980s. Although a craterlike surface roughness was formed under specific film process conditions, the formation mechanism and the controlling method of the craterlike film surface are yet to be clarified. In this report, we demonstrated a new hypothesis for the craterlike film surface roughness formation mechanism by analyzing the morphology of the surface layer of polypropylene (PP) sheets and by investigating the relationship between the surface structural changes and the changes in the entire structure. As a result, we found that an overcritical crystallization time was needed to form the crater on the surface of the BOPP film, and the crater formation mechanism was closely related not only to the surface structure changes but also to the deformation phenomenon of the spherulite in the PP sheet during stretching. Furthermore, this report shows the controlling factors in the formation of the crater structure from the viewpoint of the production conditions. © 2012 Wiley Periodicals, Inc. J. Appl. Polym. Sci. 000: 000–000, 2012

Key words: films; orientation; poly(propylene); (PP); surfaces

INTRODUCTION

Polypropylene (PP) is one of the most popular thermoplastic resins and is produced at a rate of about 42 million tons per year around the world.[1] It is a well-known fact that there are some crystal types of PP with different crystal systems, and the surface roughnesses of biaxially oriented polypropylene (BOPP) films have been investigated in association with crystal types.[2–8] Many basic studies have been reported on the formation of α and β crystals.[9–14] Natta and Corradini[9] reported in their paper in 1960 that the unit lattice of the α crystal is the monoclinic system, and now, it is known to be the most dominant crystal in PP. The β crystal was discovered by Keith et al. in 1959, and the unit lattice is a hexagonal system.[10] It was reported that β crystals are formed easily by the addition of a β nucleator into raw PP[11] under a controlled temperature gradient[12] and under a strong shear stress in an extruder, such as at a low extruding temperature.[13] In addition to these studies, the characteristics of β crystals were reported, and it was found that they have lower densities and melting temperatures (T_m's) than α crystals.[9]

It was also reported that the formation of a craterlike surface roughness in BOPP films is due to the crystal dislocation system. Because β crystals with lower densities change into α crystals with higher densities after the sheets, which contain both α and β crystals, are stretched, craters form where the β crystals existed. To obtain a craterlike surface roughness in BOPP films, Fujiyama et al.[3] reported that the stretching temperature in the machine direction (MD) process should be controlled between the T_m's of both the β and α crystals. It was also reported that the stretching temperature in the transverse direction (TD) process should be controlled between 150 and 155°C because the craters became unclear in the roughened BOPP film at a temperature lower than 150°C, and the craters disappear when it is melted at a temperature higher than 155°C.[4] On the other hand, although Fujiyama et al.[5] reported the difference in the surface roughness between a BOPP film produced by the sheet with an α nucleator and that with a β nucleator, the relationship between the crater shape and β crystals with regard to parameters such as amount and shape has not yet been

Correspondence to: S. Tamura (satoshi1.tamura@primepolymer.co.jp).

TABLE I
Properties of the PP resin

Properties	Unit	PP-A
Melt flow rate	g/10 min	3.5
mmmm	mol %	96
T_m	°C	164
ΔH_m	J/g	105
T_c	°C	115
M_w/M_n	—	5.1

clarified.[5] It was reported that there was a good relationship between the chill-roll temperature and the average roughness of the BOPP film surface, which is a parameter of crater depth, but the relationship between the chill-roll temperature and the crater diameter is yet not clear.[6] From these reports, the crater formation mechanism of BOPP films has not yet been clarified because these reports have only focused on the β crystals.

Various studies have reported changes in the crystal structure during the stretching process.[15–23] Although Koike and Cakmak[15] reported a change in the PP crystal structure during uniaxial stretching, observed by the birefringence technique, and Phillips and Nguyen[16] made a report on the relationship between the stretching stress and the change in morphology of the PP sheet,[16] no information related to surface structure has been reported. Kanai and coworkers[17–20] reported on PP spherulite deformation and crystalline orientation during stretching in terms of the stretching stress pattern and on the analytical results of the crystal structural changes observed by birefringence, light scattering, and small-angle X-ray scattering. Kanai and coworkers[21–23] also reported that there was a strong relationship between the observation results of crystal structures in PP sheets and the simulation results obtained by cooling calculations conducted with regard to the thermal transfer characteristics of PP sheets with the chill-roll cooling system. Although it was concluded in the report that the cooling simulation is an efficient method for controlling the crystallization of a PP sheet, which is an important factor in the stretchability of BOPP, there was no information on the surface structure of BOPP.

It was found in our previous study[24] that the craterlike structures on the BOPP film surface were related to the morphology of the surface layer of the PP sheets. However, even though it is an important factor in the formation of the craterlike structure of BOPP, the method for controlling the morphology of the PP sheet has not yet been discussed. The relationship between the changes in the surface structure and the whole structure has not yet been discussed either. Therefore, in this report, we give some perspective on the formation mechanism of the craters with regard to controlling the morphology of the surface layer of the PP sheet and also on its connection to changes in the entire structure.

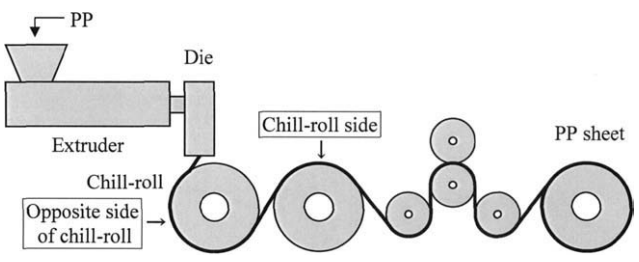

Figure 1 Schematic diagram of the PP sheet-forming machine.

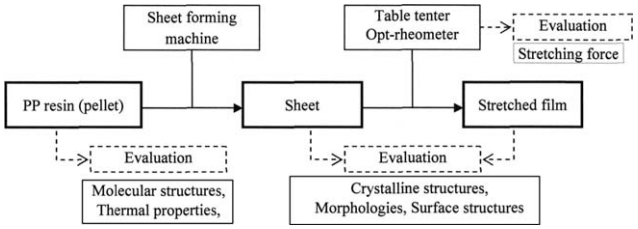

Figure 2 Diagram production and evaluation methods of each sample.

EXPERIMENTAL

Samples

To clarify the mechanism of the formation of surface craters, PP-A polymerized by Ziegler-Natta catalyst with a high tactility and a meso pentad mmmm value, which is a parameter of the isotactic index measured by ^{13}C-NMR,[25] of 96 mol % was prepared. The thermal properties of T_m, melting enthalpy (ΔH_m), and crystallization temperature (T_c) were measured by differential scanning calorimetry (DSC; PerkinElmer, Waltham Massachusetts, USA, B014-3018/B014-3003), and the molecular weight distribution parameter [weight-average molecular weight/number-average molecular weight (M_w/M_n)] was measured by gel permeation chromatography. The properties of PP-A are shown in Table I.

PP sheets were produced with a sheet-forming machine (GM Engineering, Yokohama, Japan) with an extruder diameter of 35 mm (Fig. 1). The PP resin was extruded from a T-die with a width of 200 mm at 250°C. It was cast by a chill-roll with a diameter of 250 mm at a speed of 0.8 m/min, and PP sheets with various thicknesses were produced at various chill-roll temperatures to investigate the relationship between the morphology of the PP sheets and the sheet-forming conditions. In this study, the samples were named with respect to their resin type, chill-roll temperature, and thickness. For example, sample A80–500 was the sheet made by PP-A at a chill-roll temperature of 80°C with a thickness of 500 μm. The BOPP film names are defined with an *f* at the end of the PP sheet names, for example, A80–500f.

TABLE II
Analysis Methods for the PP Sheets and Films

Sample	Analysis method	Properties obtained from the measurements
Sheets	Optical microscopy	Sectional structures (size of the crystal grain and spherulite)
	DSC	Thermal properties (T_m, ΔH_m)
	WAXD	Crystalline structures (χ_c, K)
	Light scattering	Crystalline structures (U_{max})
Films	SEM	Crater shape (diameter)
	Shape-measuring machine	Crater shape (depth, R_z)

Figure 2 shows the schematic diagram for the production and evaluation methods of the samples. After the PP sheets were cut into square shapes 85 × 85 mm^2 in size, they were stretched to BOPP films by a table tenter (Bruckner, Tokyo, Germany, KARO IV) to analyze the surface structure. After they were preheated at a definite temperature for 1 min, they were stretched at maximum stretching ratio of five times to the MD at first and then seven times to the TD. The PP sheets were also stretched by an opt rheometer (Orc Manufacturing Co., Ltd., Tokyo, Japan) to analyze the crystal structural changes. PP sheets with a rectangular shape 25 × 10 mm^2 were stretched to the MD at a stretching ratio of five times at a strain speed of 28.6%/s after they were preheated at 159°C for 5 min. The stretching force was measured by a load cell, which was equipped on a chuck of the opt rheometer with maximum load of 100 N.

Evaluation of the PP sheets and the BOPP films

The analysis methods of the PP sheets and BOPP films and the properties obtained from these measurements are shown in Table II. The sectional structures of the PP sheets were observed by an optical microscope (Nikon, Tokyo, Japan, ECLIPSE-LV100POL). When we observed the morphologies of the PP sheet with the sectional view of an optical microscope, the crystal sizes were measured by visual inspection from pictures taken with a polarizing lens. The thermal properties, T_m and ΔH_m, of the PP sheets were measured by DSC (PerkinElmer, Waltham Massachusetts, USA, B014-3018/B014-3003) at a heating rate of 10°C/min.

X-ray diffraction was conducted on the PP sheets with a Rigaku Denki, Tokyo, Japan, RINT-2500 diffractometer with Ni-filtered Cu Kα radiation. The crystallinity (χ_c) and β-crystal content (K) values of the PP sheets were calculated from the X-ray diffraction curves.[26,27] The change in the crystal structure during stretching was analyzed by light-scattering data obtained by the opt rheometer with a high-power He–Ne laser. The spherulite size (U_{max}) of the PP sheet was calculated from eq. (1), obtained by the Hv scattering pattern, which reflected the scattering of the polymer superstructure:

$$U_{max} = \frac{4.09}{(4\pi/\lambda)\sin\ \theta_{max}} \quad (1)$$

where λ is the wavelength of the He–Ne laser (632.8 nm) and θ_{max} is the scattering angle, which indicates the yield point of the scattering intensity to 45° against a plane of polarization.

The surface structures of the BOPP films were observed by scanning electron microscopy (SEM; JEOL, Tokyo, Japan, JSM5600LV). Samples were sputtered with gold in a vacuumed atmosphere, and the crater diameters were measured by visual inspection from photographs. In addition, the shapes of the craters were measured by a highly precise shape-measuring machine (Kosaka Laboratory, Tokyo, Japan, SURFCODER ET4000A) with a diamond head at a head pressure of 70 μN. The ten-point average roughness (R_z) defined by JIS B0601 (1994) was used as the parameter of depth of the crater on the BOPP film surface.

Moreover, to investigate the crater formation mechanism at the surface layer of PP sheet, the influence of cooling speed was studied at the sheet-forming condition described at section 2.1). The temperature of PP resin starts to drop after PP sheet is extruded from the die and touches the chill roll. PP crystallization starts when the sheet temperature reaches T_c at 115°C in the case of PP-A. After sheet temperature is kept at T_c until the latent heat is consumed, the sheet temperature starts to drop again. Crystallization time is defined as the time during which PP sheet temperature is kept at T_c, and PP crystallizes during the crystallization time. In this report, it is assumed that heat is conducted by primary thermal conduction expressed in eq. (2) and is transferred at the boundary condition expressed in eq. (3):

$$\frac{\partial T}{\partial t} = \frac{k}{c_p \rho} \times \frac{\partial^2 T}{\partial x^2} \quad (2)$$

$$k\frac{\partial T}{\partial x} = h(T_w - T_\infty) \quad (3)$$

where T is the sheet temperature (K), t is time (s), k is the thermal conductivity (0.28 W m^{-1} K^{-1}), C_p is the heat capacity (1.93 J kg^{-1} K^{-1}), ρ is the density

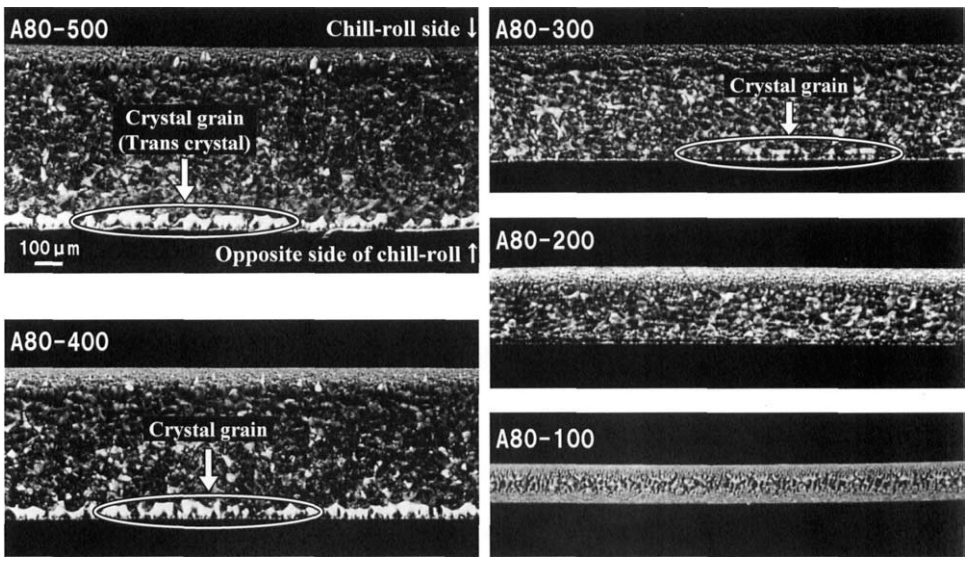

Figure 3 Optical microscopy images of PP sheets with different thicknesses.

of PP, x is the sheet position from the chill roll (m), h is the heat-transfer coefficient (756 W m^{-2} K^{-1}), T_w is the surface temperature of the sheet (K), and T_∞ is the chill-roll temperature (K). Although the density of PP depends on the temperature, the fixed value 890 kg/m^3 was used in this study to make the calculation simple. The heat-transfer coefficient was determined by measurement of the real temperatures of the chill roll and PP sheet with a touch-type thermometer.

RESULTS AND DISCUSSION

Influence of the sheet-forming conditions on the crater formation of the BOPP film

First, the influence of the thickness of the PP sheets on the crater structure was studied. Figure 3 shows the polarized micrographs of the cross-sectional views of the PP sheets in the MD and the normal direction. As for the A80–500 sheet, a number of white grains were observed only in the surface layer of the opposite side of the chill roll. Because the amorphous parts are not portrayed in white on a polarizing microscope, these white grains were considered to be β crystals of PP[4] and also transcrystals.[28,29] Although these white crystal grains were observed even in the A80–400 and A80–300 sheets, with thicknesses of 400 and 300 μm, respectively, they were not observed in the A80–200 and A80–100 sheets, with thicknesses of 200 and 100 μm, respectively. Figure 4 shows the relationship between the shapes of the crystal structure and the thickness of the PP sheet. As a result, although the crystal grains were not observed in the surface layer of the chill-roll side, the crystal grain size (depth and diameter) in the surface layer of the opposite side of the chill

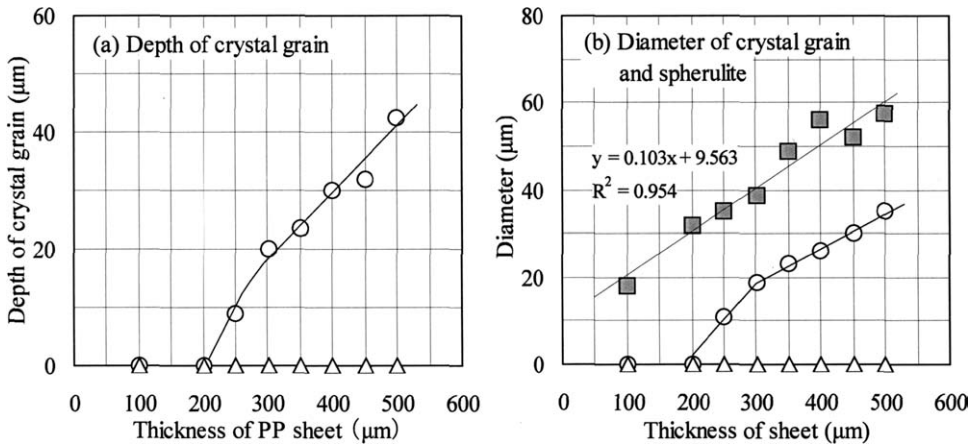

Figure 4 Crystal structure of PP sheets with different thicknesses: (○) crystal grain on the surface layer of the opposite side of the chill roll, (△) crystal grain on the surface layer of the chill-roll side, and (■) spherulite in the central part of the sheet.

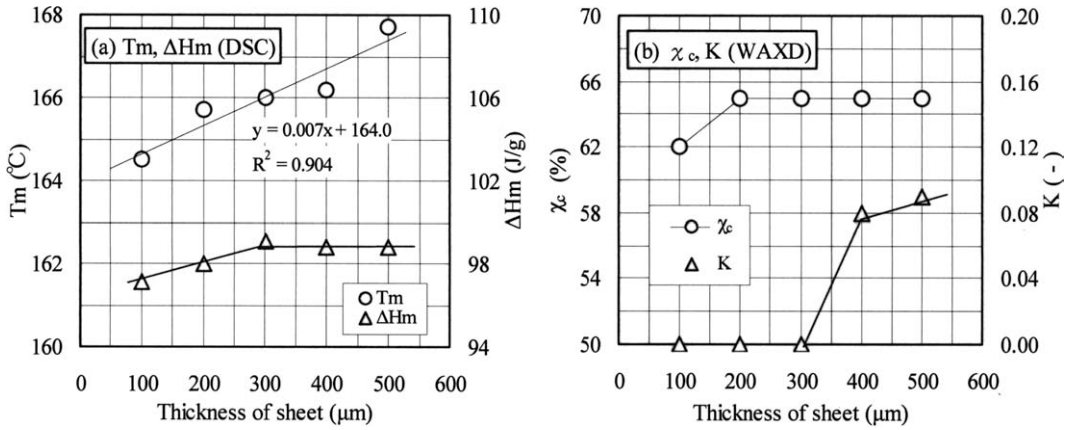

Figure 5 Properties of PP sheets with different thicknesses as measured by (a) DSC and (b) WAXD.

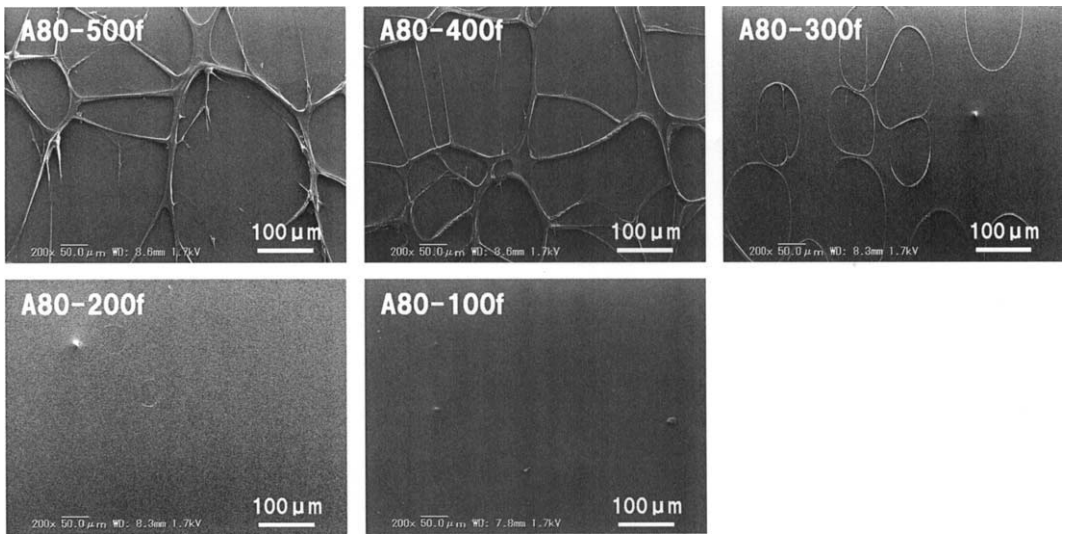

Figure 6 SEM images of the BOPP films on the opposite side of the chill roll obtained from PP sheets with different thicknesses.

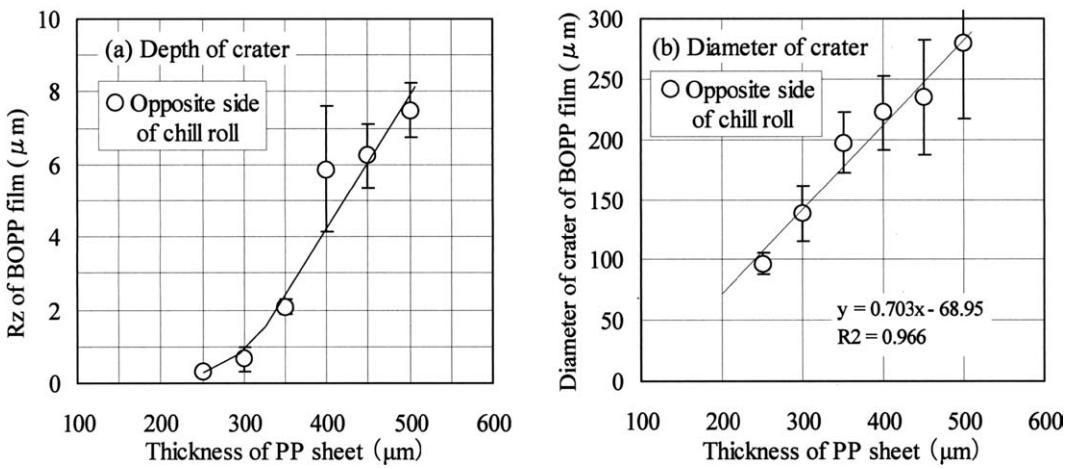

Figure 7 Relationship between the PP sheet thickness and the crater shape.

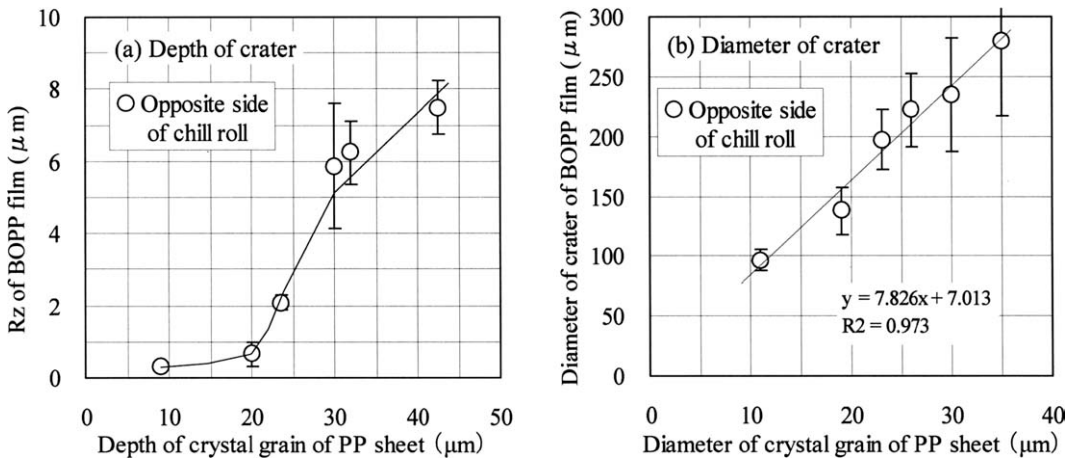

Figure 8 Relationship between the crystal structure of the PP sheets and the crater structure of the BOPP films.

roll became larger as the PP sheet became thicker than 200 μm, whereas the size of the spherulite in the center of the PP sheet got larger as the PP sheet became thicker from 100 μm.

To examine this more deeply, the PP sheet was analyzed by DSC and wide-angle X-ray diffraction (WAXD). T_m gradually increased from 164.5 to 167.7°C as the PP sheet thickened [Fig. 5(a)]. Because T_m is closely related to the thickness of lamella,[29] the result indicates that the lamella became thicker with the increase in PP sheet thickness. ΔH_m increased slightly as the thickness of the PP sheet increased from 100 to 300 μm and was saturated from 300 to 500 μm [Fig. 5(a)]; this was in accordance with the behavior of χ_c measured by WAXD [Fig. 5(b)]. Furthermore, β crystals were detected at thicknesses of the PP sheet of 400 μm or greater.

Next, the surface structures of the BOPP films obtained by the stretching of PP sheets with different thicknesses were observed (Fig. 6). Clear crater structures were observed on the opposite side of the chill roll of the BOPP films obtained from the PP sheets with thicknesses from 500 to 300 μm. Crater structures were not observed on the BOPP films obtained from the A80–200 and A80–100 sheets or on the chill-roll sides of all of the samples. These results show an adequate relationship between the existences of the crystal grains on the PP sheets and the formation of craters on the BOPP films. Figure 7 shows the relationship between the crater shape and the thickness of PP sheets. The crater shape indicated an adequate relationship with the thickness of the PP sheet. Figure 8 shows the relationship between the crystal grain structure of the PP sheets and the crater structure of the BOPP films. Because there was also a good relationship between the crystal grain structure and the crater structure, we assumed that the formation mechanism of the crater was related to the crystal deformation.

These results indicate that crater shape could be controlled by the white crystal grain size, which was influenced by the thickness of the PP sheet. To examine this more deeply, the sheet temperatures at several distances from the surface of the opposite side of the chill roll were simulated by eqs. (2) and (3). Figure 9(a) shows the calculated results of A80–500 at intervals of 100 μm, where 0 μm indicates the surface of the opposite side of the chill roll and 500 μm indicates the surface of the chill-roll side. From these results, we observed that the temperature of the chill-roll side dropped more quickly than that of the opposite side of the chill roll. To investigate the influence of the thickness of PP sheet on the sheet surface temperature, the calculated results of the primary sheet temperatures of the opposite side of the chill roll and the chill-roll side are shown in Figure 9(b,c), respectively. A flat area at a T_c of 115°C was observed on the opposite side of the chill roll of A80–500, but no flat area was observed on either side of A80–100. These flat areas, from 106 to 124°C, were defined as the crystallization time, and the relationship between the calculated results of the crystallization time and the crystal grain sizes are shown in Figure 9(d). As a result, we found that there was an adequate relationship between them. Furthermore, the relationship between the crystallization time and the crater formation was investigated [Fig. 9(e)]. From these results, we found that a crystallization time of greater than 1.5 s was required to create the crystal grain and crater on the BOPP films on the opposite side of the chill roll in our experimental method, and this study, with regard to the thickness of the PP sheet, was not discussed in previous reports.

Next, the influence of the chill-roll temperature on the crater structure was studied. Figure 10 shows the polarized micrographs of the cross-sectional views of the PP sheets in the MD and the normal direction.

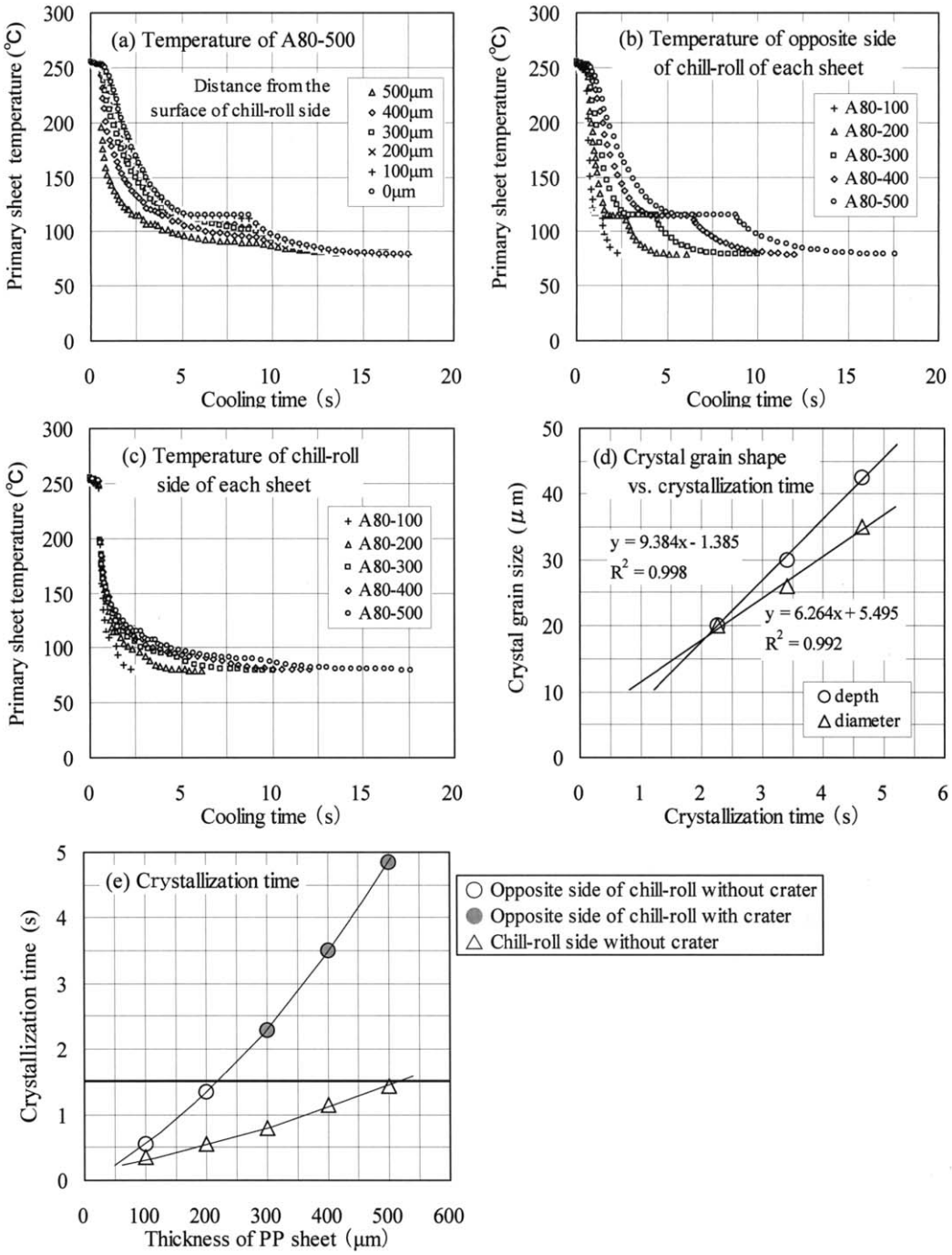

Figure 9 Calculated results of the temperature of the PP sheets with different thicknesses (conditions: die temperature = 250°C, chill-roll temperature = 80°C, stretching temperature = 159°C, MD/TD stretching ratio = 5/7).

Crystal grains were not observed in the surface layer of either side of the chill roll with chill-roll temperatures ranging from 30 to 65°C. On the other hand, many crystal grains were formed in the surface layer of the opposite side of the chill roll from A80–300 to A95–300 sheets with chill-roll temperatures from 80 to 95°C, and they became larger with increasing chill-roll temperature (Fig. 11). Furthermore, crystal grains in the surface layer of the chill-roll side were observed with chill-roll temperatures at and above 90°C, although they were not observed in the surface layer of the A80 sheets cast at 80°C with several thicknesses, from 500 to 100 μm.

Figure 12 shows the melting properties and crystal structures measured by DSC and WAXD. Because T_m and ΔH_m increased as the chill-roll temperature increased, we assumed that the thickness of the lamella and the amount of the crystal part increased with increasing chill-roll temperature or, in other words, with slow cooling [Fig. 12(a)]. As proof, χ_c

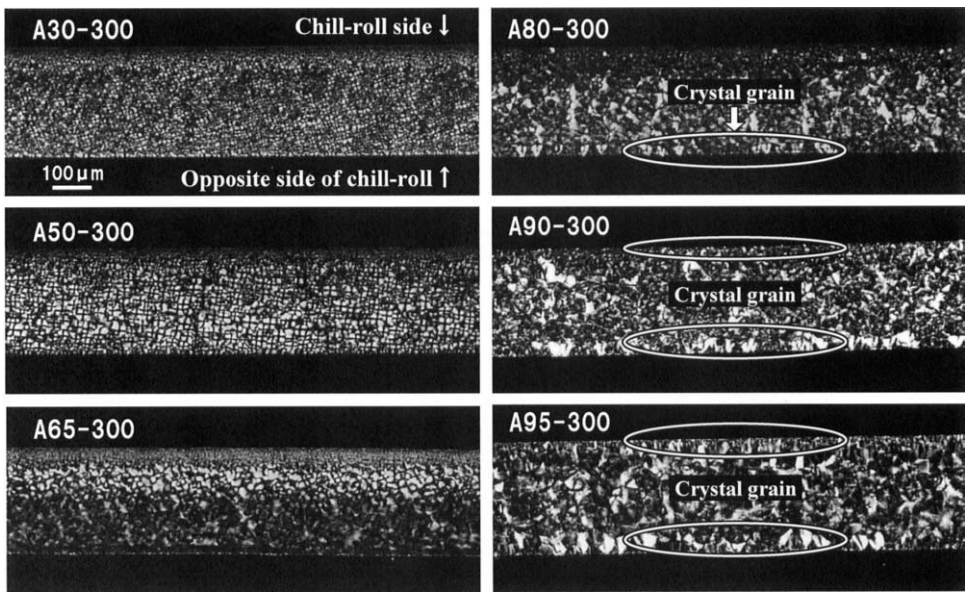

Figure 10 Optical microscopy images of the PP sheets with different chill-roll temperatures.

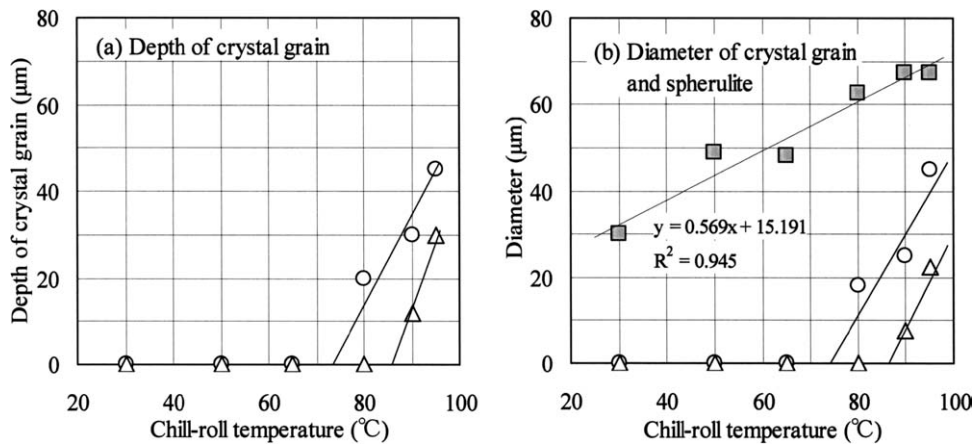

Figure 11 Crystal structure of PP sheets with different chill-roll temperatures: (○) crystal grain on the surface layer of the opposite side of the chill roll, (△) crystal grain on the surface layer of the chill-roll side, and (■) spherulite in the central part of the sheet.

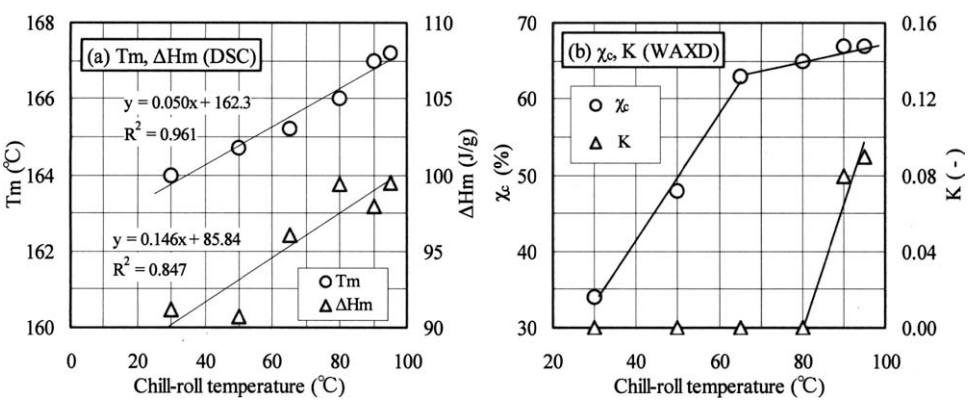

Figure 12 Properties of PP sheets with different chill-roll temperatures measured by (a) DSC and (b) XRD.

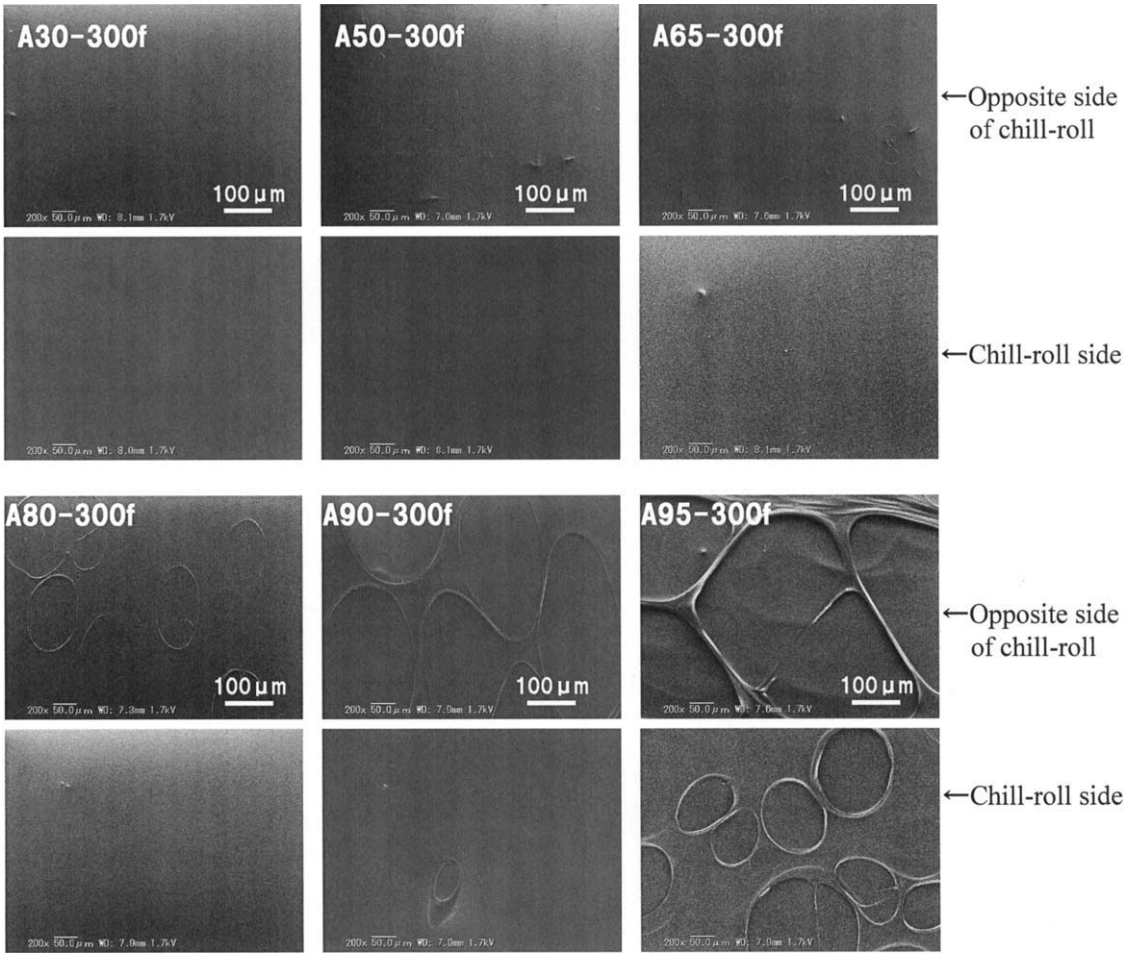

Figure 13 SEM images of BOPP film surfaces obtained from PP sheets with different chill-roll temperatures.

increased with increasing chill-roll temperature [Fig. 12(b)]. Furthermore, β crystals were detected at and above the chill-roll temperature of 90°C.

Figure 13 shows the SEM images of the surfaces of the BOPP films obtained from PP sheets with different chill-roll temperatures. Although crater structures were not observed on the surface of the opposite side of the chill roll of the A30–300f to A65–300f films, they were observed in the A80–300f to A95–300f films. Additionally, they were observed on the surface of the chill-roll side, too, from A90–300f to A95–300f, in which crystal grains in the surface layer of the chill-roll side were observed in the PP sheets. From these results, a higher chill-roll temperature is required to produce craters on the BOPP film surface of the chill-roll side. Furthermore, crystal grains in the PP sheet are needed to produce craters on the BOPP film.

To investigate the influence of the chill-roll temperature on the sheet surface temperature, the calculated results of the primary sheet temperatures of the opposite side of the chill roll and chill-roll side are shown in Figure 14(a,b), respectively. The crystallization time became longer as the chill-roll temperature became higher. This graph shows that a crystallization time of more than 1.5 s was needed to create the crater on the surface of the BOPP film with our experimental method. This results obtained from the PP sheet with the different chill-roll temperatures were similar to those of PP sheets of different thicknesses. It was confirmed that crater formation could be controlled by the crystallization time, which was a function of the thickness of the PP sheet and the chill-roll temperature. In addition, craters could be formed on the BOPP film surface of the chill-roll side when we controlled the crystallization time suitably, whereas previous reports discussed only the cases of the crater on the surface of the opposite side of the chill roll.

Relationship between the surface structure and the whole structure of the BOPP film

To study the crater formation mechanism, PP sheets cast at different chill-roll temperatures of A80–300 with a high χ_c of 65% and A30–300 with a low χ_c of 34% measured by WAXD were stretched by the opt rheometer, which gave information on the

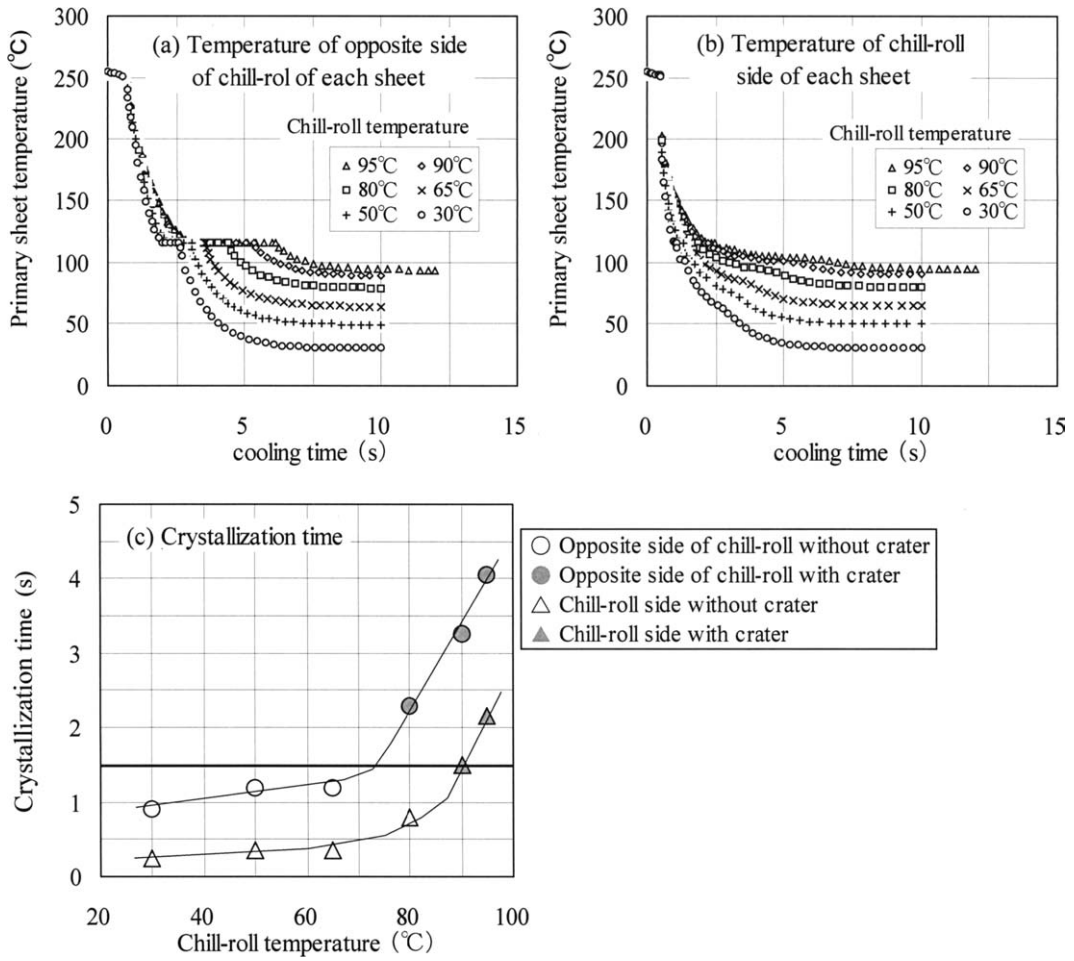

Figure 14 Calculated results of the temperature of the PP sheets with different chill-roll temperatures (conditions: die temperature = 250°C, thickness of the PP sheets = 300 μm, stretching temperature = 159°C, MD/TD stretching ratio = 5/7).

superstructure during stretching. Figure 15 shows the change of the surface roughness parameter (R_z) value with the stretching ratio. Although the R_z of A80–300 was larger than that of A30–300, the R_z values of both samples had a yield point at a stretching ratio of 2 times, and R_z gradually decreased as the stretching ratio increased. The reason for this was that the deep dent that was obtained in the early stage of the stretching process changed to a shallow crater with cutting through a thick wall at stretching ratios of 2 times or higher, as mentioned in our previous report.[24] In other words, despite the fact that the crystal grains were formed in the surface layer uniformly, the deformation of the surface structure started partially as the weak parts were stretched first. These results coincide with the results obtained by the stretching test with the table tenter and were assumed to be caused by the difference in crystal grain size between the sheets.

Figure 16 shows the change in the light-scattering pattern with the stretching ratio. A80–100 was used instead of A80–300 because the light-scattering peak of A80–300 was too week for data analysis. The

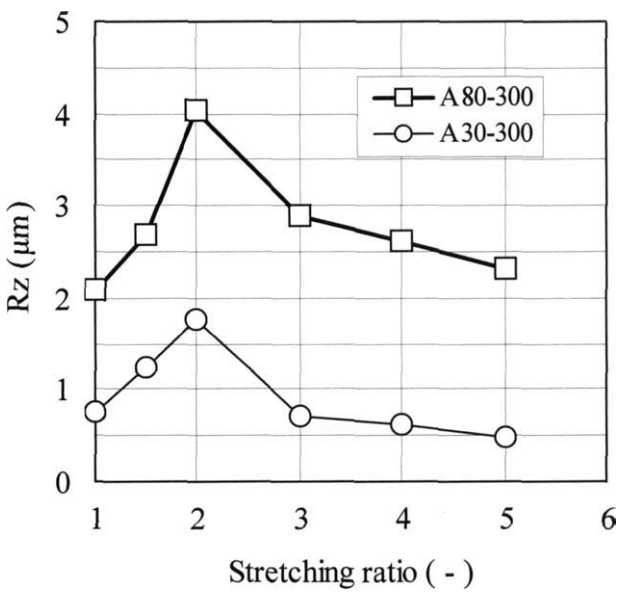

Figure 15 R_z values of the BOPP films stretched by the opt rheometer obtained from PP sheets with different chill-roll temperatures.

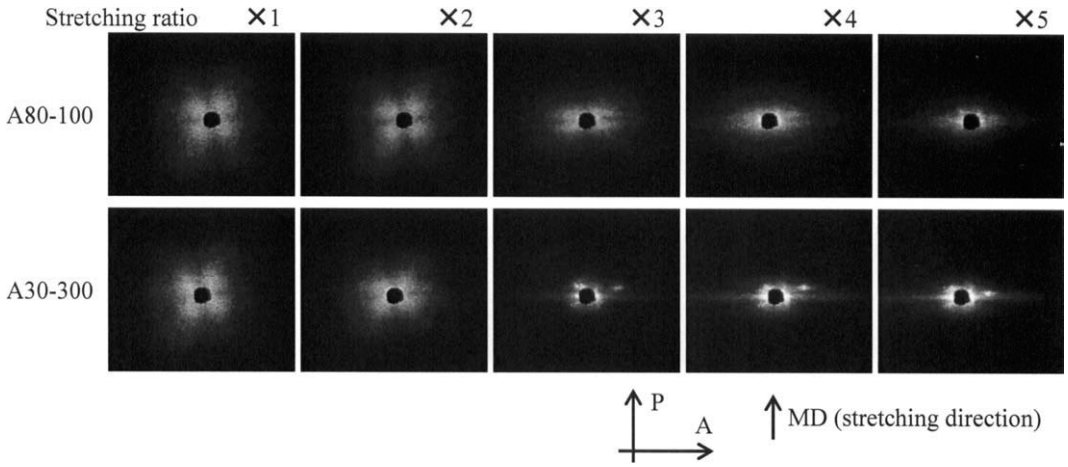

Figure 16 Light-scattering patterns stretched by the opt rheometer obtained from PP sheets with different chill-roll temperatures (P = polarizer, A = analyzer).

light-scattering patterns of the unstretched sheets of both samples showed clear clover patterns, and this demonstrated the existence of spherulites. There were no considerable changes in the light-scattering pattern at a stretching ratio of 2 times, and the spherulites still remained in the PP sheet (Table III). The spherulites were destroyed at higher stretching ratios because the clover pattern changed to a streak pattern in the equatorial direction. This result indicates that a partial deformation of the spherulite was observed at the stretching ratio lower than 2 times, and the crystal structure changed totally at higher stretching ratios. Although the sizes of the crystal grains of these two PP sheets were different, the deformation patterns of the spherulites were similar in these two PP sheets. Because the stretching ratio with the maximum R_z value and that of the existence limit of the spherulite was the same, we concluded that the crater formation on the BOPP film surface was closely related to the spherulite deformation of the entire BOPP film.

CONCLUSIONS

The formation mechanism of the craterlike surface roughness of BOPP films was investigated. It was found that the thickness of the PP sheet had a great effect on the crater shape of the BOPP film because the crystal grains in the surface layer of the PP sheet changed according to the thickness of the PP sheets. The formation mechanism of the craterlike surface roughness of the BOPP film was investigated. The investigation showed that a crystallization time over a critical value was required to produce crystal grains in the surface layer of the PP sheet with β-type transcrystals.

Furthermore, the effect of the chill-roll temperature in the preceding PP sheet was investigated. It was found that crystal grains in the surface layer were easily created at higher chill-roll temperatures. From the analysis of the cooling calculation, it was confirmed that more than 1.5 s of crystallization time was required to produce crystal grains in the surface regions of the PP sheet. It was also found that a crater could be formed on both surfaces of the BOPP films, regardless of the sides of the chill roll, when the crystallization time was controlled for more than 1.5 s. It may be said that the technology of crater formation could be settled by the simulation of PP sheets produced under different conditions.

In addition, the crater formation mechanism was researched in terms of the stretching behavior of the entire PP sheet with an opt rheometer. The change in the surface roughness with the stretching ratio showed that the deformation of the surface structure partially started before the craters were formed on the BOPP film surface, and R_z indicated a maximum value at a stretching ratio of 2 times. In addition, it was found that the spherulites began to decay at a stretching ratio higher than 2 times through analysis of the light-scattering method. As a result, we concluded that the crater formation on the BOPP film surface was closely related to spherulite deformation and collapse of the entire BOPP film.

TABLE III
Changes in U_{max} (μm) during Stretching in the MD

	Stretching ratio	
Sheet	1	2
A80–100	4.9	5.6
A30–300	6.5	9.8

References

1. Takesue, K. Kagaku-Keizai 2011, 92, 3.
2. Fujiyama, M.; Kawamura, Y.; Wakino, T.; Okamoto, T. J Appl Polym Sci 1988, 36, 985.

3. Fujiyama, M.; Kawamura, Y.; Wakino, T.; Okamoto, T. J Appl Polym Sci 1988, 36, 995.
4. Fujiyama, M.; Kawamura, Y.; Wakino, T.; Okamoto, T. J Appl Polym Sci 1988, 36, 1011.
5. Fujiyama, M.; Kawamura, Y.; Wakino, T.; Okamoto, T. J Appl Polym Sci 1988, 36, 1025.
6. Fujiyama, M.; Kawamura, Y.; Wakino, T.; Okamoto, T. J Appl Polym Sci 1988, 36, 1035.
7. Fujiyama, M.; Kawamura, Y.; Wakino, T.; Okamoto, T. J Appl Polym Sci 1988, 36, 1049.
8. Fujiyama, M.; Kawamura, Y.; Wakino, T.; Okamoto, T. J Appl Polym Sci 1988, 36, 1061.
9. Natta, G.; Corradini, P. Nuovo Cimento Suppl 1960, 15, 40.
10. Keith, H. D.; Padden, F. J.; Walter, N. M.; Wickoff, H. W. J. Appl Phys 1959, 30, 1485.
11. Asano, T.; Fujiwara, Y. Polym J 1979, 11, 383.
12. Meille, S. V.; Ferro, D. R.; Bruckner, S.; Lovinger, A. J.; Padden, F. J. Macromolecules 1994, 27, 2615.
13. Moitzi, J.; Skalicky, P. Polymer 1993, 34, 3168.
14. Farah, M.; Bretas, R. J Appl Polym Sci 2004, 91, 3528.
15. Koike, Y.; Cakmak, M. Polymer 2003, 4249, 44.
16. Phillips, R. A.; Nguyen, T. J Appl Polym Sci 2001, 80, 2400.
17. Sakauchi, K.; Uehara, H.; Yamada, T.; Obata, Y.; Takebe, T.; Kanai, T. Presented at the 21st Polymer Processing Society Annual Meeting, Leipzig, Germany, 2005.
18. Kanai, T.; Matsuzawa, N.; Takebe, T.; Yamada, T. Polymer Processing Society Regional Meeting Europe CD-ROM Abstracts; Gothenburg, Sweden, 2007.
19. Kanai, T.; Matsuzawa, N.; Yamaguchi, H.; Takebe, T.; Yamada, T. 24th Polymer Processing Society Annual Meeting CD-ROM Abstracts; Salerno, Italy, 2008.
20. Kanai, T.; Takebe, T.; Matsuzawa, N.; Yamaguchi, H. Presented at the Asian Workshop on Polymer Processing, Penang, Malaysia, 2009.
21. Kanai, T.; Yonekawa, F.; Kuramoto, I. 17th Polymer Processing Society Annual Meeting Abstracts; Montreal, Canada, 2001; p 82.
22. Kanai, T.; Seikei-Kakou 2006, 18(1), 53.
23. Matsuzawa, N.; Kamatani, Y.; Kanai, T.; Yamada, T.; Sakauchi, K.; Uehara, H. 22th Polymer Processing Society Annual Meeting CD-ROM Abstracts; Yamagata, Japan, 2006.
24. Tamura, S.; Ohta, K.; Kanai, T. J Appl Polym Sci 2012, 124, 2725.
25. Zambelli, A.; Locatelli, P.; Bajo, G.; Bovey, F. A. Macromolecules 1975, 8, 687.
26. Natta, G.; Corradini, P.; Cesari, M. Rend Accad Naz Lincei 1957, 22, 11.
27. Tuner-Jones, A.; Aizilewood, J. M.; Beckert, D. R. Makromol Chem 1964, 75, 134.
28. Yamakita, T. T. IEE Jpn 1997, 117-A, 12.
29. Bailey, G. W. J Polym Sci 1962, 241, 62.